

Light-shining-through-wall cavity setups for probing ALPs

Dmitry Salnikov^{a,b,*} and Dmitry Kirpichnikov^a

^a*Institute for Nuclear Research of the Russian Academy of Sciences,
60th October Anniversary Prospect, 7a, 117312 Moscow, Russia*

^b*Moscow State University,
Leninskiye Gory, 119991 Moscow, Russia*

E-mail: salnikov.dv16@physics.msu.ru, kirpich@ms2.inr.ac.ru

We study potential probing of axion-like-particles (ALPs) with Light-Shining-through-Wall (LSW) experimental facilities which consist of two radio-frequency cavities. We compare the efficiencies of four cavity designs, involving the pump modes and external magnetic fields. In addition, we study in detail the ALP sensitivity dependence both on the relative position of cavities and on their aspect ratio.

*International Conference on Particle Physics and Cosmology (ICPPCRubakov2023)
02-07, October 2023
Yerevan, Armenia*

*Speaker

1. Introduction.

Light feebly-interacting pseudoscalar particles appear in modern particle physics in various ways. Originally, a pseudoscalar particle called an axion was proposed in late 1970s to explain the strong CP problem in quantum chromodynamics [1, 2]. In addition to the motivation for the particle physics models, axions and ALPs are of a great interest in cosmology because they could make up a significant fraction of the dark matter in the Universe [3–5].

The Lagrangian for interacting ALPs and photons can be written as follows

$$\mathcal{L} = -\frac{1}{4}F_{\mu\nu}F^{\mu\nu} + \frac{1}{2}\partial_\mu a \partial^\mu a - \frac{1}{2}m_a^2 a^2 - \frac{1}{4}g_{a\gamma\gamma} a F_{\mu\nu}\tilde{F}^{\mu\nu}, \quad (1)$$

where $F_{\mu\nu}$ is the electromagnetic tensor and $\tilde{F}^{\mu\nu} = \frac{1}{2}\epsilon^{\mu\nu\alpha\beta}F_{\alpha\beta}$ is its dual, a is the ALP field of mass m_a with dimensionful photon-axion coupling $g_{a\gamma\gamma}$.

A typical strategy for probing ALPs implies both their production and detection in a laboratory, and usually called Light-Shining-through-Wall (LSW) experiments [6–9]. The LSW setups consist of two cavities separated by a non-transparent wall. ALPs are produced in the first cavity by interaction of electromagnetic field components. Generated ALPs can pass through the wall and convert back to photons in the detection cavity. Recently, several proposals with LSW radio cavities appeared in the literature including superconducting radio frequency (SRF) cavities [10–12]. In this paper we compare four different LSW cavity setups including modification of the CROWS [9, 13].

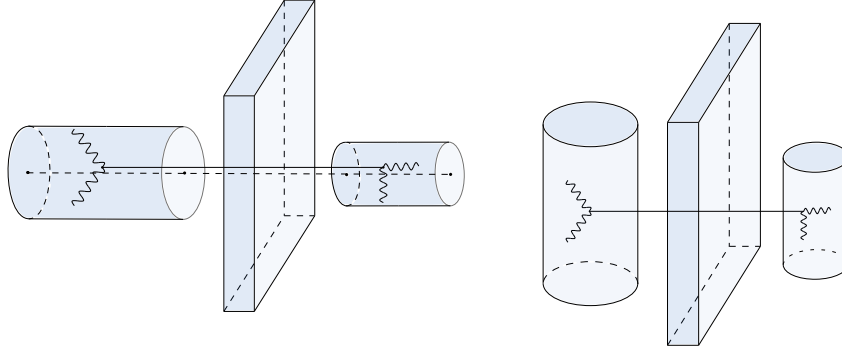


Figure 1: Two specific types of the experimental configuration consisting of two cylindrical cavities with (left panel) coaxial or (right panel) parallel orientation and screened by axion-penetrable wall. Wavy and solid lines represent electromagnetic field (cavity mode or magnetic field) and ALPs respectively.

We also study transfer of ALPs from the emitter to the receiver for the specific designs and discuss their optimal configuration, either coaxial or parallel (see e. g. Fig. 1 for detail).

2. Axion electrodynamics.

The Euler-Lagrange equation for the ALP field reads,

$$(\partial_\mu \partial^\mu + m_a^2) a = -\frac{1}{4}g_{a\gamma\gamma} F_{\mu\nu}\tilde{F}^{\mu\nu}, \quad (2)$$

while the Maxwell's equations with an ALP-induced current read,

$$\partial_\mu F^{\mu\nu} = -g_{a\gamma\gamma} \partial_\mu a \tilde{F}^{\mu\nu} . \quad (3)$$

One can rewrite Eqs. (2) and (3) in terms of the electric and magnetic fields,

$$(\partial_\mu \partial^\mu + m_a^2) a = g_{a\gamma\gamma} (\vec{E} \cdot \vec{B}) , \quad (4)$$

$$(\vec{\nabla} \cdot \vec{E}) = \rho_a , \quad [\vec{\nabla} \times \vec{B}] = \dot{\vec{E}} + \vec{j}_a , \quad (5)$$

where the density of charge ρ_a and current \vec{j}_a are respectively given by

$$\rho_a = -g_{a\gamma\gamma} (\vec{\nabla} a \cdot \vec{B}) , \quad \vec{j}_a = g_{a\gamma\gamma} ([\vec{\nabla} a \times \vec{E}] + \dot{a} \vec{B}) . \quad (6)$$

3. The emitter cavity.

We consider two options for the production of ALPs using RF cavities:

(i) a normally conducting RF cavity with a single pump mode with frequency ω_0 immersed in a strong static magnetic field \vec{B}_{ext} . We use the notation **MF emitter** (i. e. pump mode (**M**) + magnetic field (**F**)) for this case throughout the paper;

(ii) a superconducting RF cavity with two pump modes at frequencies $\omega_{1,2}$. We use notation **MM emitter** (pump mode (**M**) + pump mode (**M**)) for this setup.

For the MF emitter case, the source function in the Eq. (4) contains a single component oscillating at the frequency $\omega_a = \omega_0$. However, for the MM emitter case, there are two components at frequencies $\omega_a = \omega_\pm = \omega_2 \pm \omega_1$ ($\omega_2 > \omega_1$). Each particular combination of the field for both MF emitter and MM emitter reads,

$$f(t, \vec{x}) = g_{a\gamma\gamma} E_0^{\text{em}} B_0^{\text{em}} \text{Re} \left[(\vec{\mathcal{E}} \cdot \vec{\mathcal{B}})(\vec{x}) \cdot e^{-i\omega_a t} \right] , \quad (7)$$

where $E_0^{\text{em}}, B_0^{\text{em}}$ are typical values of the emitter EM fields, $(\vec{\mathcal{E}} \cdot \vec{\mathcal{B}})(\vec{x})$ is a dimensionless function determined by the production approach. It is worth noticing that Eq. (4) implies the following solution,

$$a(t, \vec{x}) = g_{a\gamma\gamma} E_0^{\text{em}} B_0^{\text{em}} \int_{V_{\text{em}}} d^3x' \text{Re} \left[(\vec{\mathcal{E}} \cdot \vec{\mathcal{B}})(\vec{x}') \right. \\ \left. \times \frac{e^{ik_a |\vec{x} - \vec{x}'| - i\omega_a t}}{4\pi |\vec{x} - \vec{x}'|} \right] \equiv \text{Re} [a(\vec{x}) e^{-i\omega_a t}] , \quad (8)$$

where $k_a = \sqrt{\omega_a^2 - m_a^2}$ are typical momenta of the produced ALPs, integration is performed over the emitter volume V_{em} . One can replace ik_a with $-\kappa_a = -\sqrt{m_a^2 - \omega_a^2}$ in Eq. (8) for $m_a \gtrsim \omega_a$.

4. The receiver cavity.

A resonant generation of electromagnetic modes in the detecting cavity caused by the axion-induced current (see Eqs. (6) for detail). Two options are assumed for detection:

(i) the receiver cavity is a normally conducting one, and it is immersed into external constant magnetic field \vec{B}_{ext} . We use the notation **M*F receiver** (induced signal mode (\mathbf{M}^*) + magnetic field (\mathbf{F}) of the receiver) for that case (the label \mathbf{M}^* denotes the mode that we expect to detect throughout the paper);

(ii) the receiver cavity is superconducting, and it is pumped by the detecting mode. We use the notation **M*M receiver** (induced signal mode (\mathbf{M}^*) + pump mode (\mathbf{M}) of the receiver) for this setup of the cavity. The typical magnitude of the signal can be characterized by the expression [10, 12]

$$G = -\frac{Q_{\text{rec}}}{\omega_s} \cdot \frac{1}{V_{\text{rec}}} \int_{V_{\text{rec}}} d^3x (\vec{E}_s^* \cdot \vec{j}_a), \quad (9)$$

where Q_{rec} is a quality factor for the receiver eigenmode and V_{rec} is the volume of the receiver cavity, ω_s is a frequency of the receiver signal eigenmode, and $\vec{E}_s(\vec{x})$ is a dimensionless signal eigenmode. Remarkable, the general expression of the overlapping integral in Eq. (9) for both M*F and M*M receivers reads

$$\int_{V_{\text{rec}}} d^3x (\vec{E}_s^* \cdot \vec{j}_a) = -i\omega_s g_{a\gamma\gamma} B_0^{\text{rec}} \int_{V_{\text{rec}}} d^3x (\vec{E} \cdot \vec{B})^*(\vec{x}) a(\vec{x}), \quad (10)$$

where B_0^{rec} is a characteristic magnetic field of the detection cavity and $(\vec{E} \cdot \vec{B})^*(\vec{x})$ is a dimensionless complex-conjugated function that is associated with a specific way of ALP detection.

5. Signal power.

Here we discuss the signal induced by the axion field for the cavity experimental setups. To be more concrete, by using Eqs. (8) and (10) we can rewrite the amplitude in Eq. (9) in general form

$$G = iQ_{\text{rec}} g_{a\gamma\gamma}^2 E_0^{\text{em}} B_0^{\text{em}} B_0^{\text{rec}} \cdot \frac{V_{\text{em}} \mathcal{G}}{\Delta}, \quad (11)$$

where Δ is typical distance between cavities, and the dimensionless factor \mathcal{G} is given by the following expression

$$\mathcal{G} = \int_{V_{\text{rec}}} \frac{d^3x}{V_{\text{rec}}} \int_{V_{\text{em}}} \frac{d^3x'}{V_{\text{em}}} (\vec{E} \cdot \vec{B})^*(\vec{x}) (\vec{E} \cdot \vec{B})(\vec{x}') \frac{e^{ik_a|\vec{x}-\vec{x}'|}}{4\pi} \frac{\Delta}{|\vec{x}-\vec{x}'|}. \quad (12)$$

The typical signal power reads

$$P_{\text{signal}} = \frac{\omega_s}{Q_{\text{rec}}} \int_{V_{\text{rec}}} d^3x \langle |\vec{E}_s(\vec{x}, t)|^2 \rangle_t = \frac{\omega_s}{Q_{\text{rec}}} \frac{1}{2} |G|^2 V_{\text{rec}}, \quad (13)$$

where $\vec{E}_s(\vec{x}, t)$ is a signal solenoidal electric field that is resonantly enhanced by the ALP in the receiver.

We estimate sensitivity numerically as maximum output in the receiver cavity that is given by the Dicke radiometer equation,

$$\text{SNR} = \frac{P_{\text{signal}}}{P_{\text{noise}}} \cdot \sqrt{t\Delta\nu}, \quad (14)$$

where t is an integration time for a signal, $\Delta\nu$ is its bandwidth and P_{noise} is a power of thermal noise which can be estimated as $P_{\text{noise}} \simeq T\Delta\nu$ in the limit $\omega_s \ll T$, where $T \simeq 1.5$ K is the typical temperature of the receiver. We consider two options for $\Delta\nu$: the bandwidth of a cavity mode itself (i.e. $\Delta\nu \simeq \nu_s/Q_{\text{rec}}$, where $\nu_s = \omega_s/(2\pi)$) and the narrowest possible bandwidth of a pump generator, which can be as small as $\Delta\nu \simeq 1/t$ (see e. g. Refs. [10, 12] and references therein).

Finally, by using Eqs. (13) and (14) we obtain the expected sensitivity,

$$g_{a\gamma\gamma} = \left[\frac{2\Delta^2 T \text{SNR}}{\omega_s Q_{\text{rec}} E_{0,\text{em}}^2 B_{0,\text{em}}^2 B_{0,\text{rec}}^2 V_{\text{em}}^2 V_{\text{rec}} |\mathcal{G}|^2} \right]^{\frac{1}{4}} \left(\frac{\Delta\nu}{t} \right)^{\frac{1}{8}}, \quad (15)$$

where signal to noise ratio is $\text{SNR} \simeq 5$ and the typical parameters are considered in the next sections.

6. The expected reach.

Now we compare the efficiencies of four different experimental setups for probing ALPs with LSW methods:

- **MF emitter + M*F receiver;**
- **MM emitter + M*M receiver;**
- **MM emitter + M*F (RF) receiver;**
- **MF emitter + M*M receiver.**

In addition, we study in detail the sensitivity dependence on the cavity location and on the aspect ratio R/L of the ALP emitter.

6.1 MF emitter + M*F receiver.

Let us consider the typical LSW setup consisting of two RF cavities which are placed both into a strong static magnetic field [9, 13]. We carry out analysis for the characteristic volume of the emitter and receiver cavities $V_{\text{rec}} = V_{\text{em}} \simeq 1 \text{ m}^3$, we also exploit the receiver quality factor $Q_{\text{rec}} \simeq 10^5$. We consider the typical magnitude of the emitter pump mode $E_0^{\text{em}} = 3 \text{ MV/m}$. The typical values of the static magnetic fields are taken to be $B_0^{\text{em}} = B_0^{\text{rec}} = 3 \text{ T}$. The distance between receiver and emitter walls is $\Delta = 0.5 \text{ m}$. The pump mode of the emitter and the signal mode of the receiver are TM_{010} .

In Fig. 2 (left panel) we show the expected sensitivity of the setup as a function of R/L for both parallel and coaxial designs of the cavities (see e. g. Fig. 1 for detail), we also set the ALP benchmark masses to be $m_a = 0$ and $m_a \simeq \omega_a$. It must be noticing that we consider sensitivity for $m_a = 0$ as the most important (optimal) setup characteristic compared to the resonant bound at $m_a = \omega_s$ regime throughout the paper. It implies that the typical bounds at $m_a = 0$ cover the larger logarithmic mass scale range ($m_a \lesssim \omega_a/2$) in $(g_{a\gamma\gamma}, m_a)$ plane.

Thus we take into account that $Q_{\text{rec}} = 10^5$ for $R/L = 1$. It turns out that coaxial design for $R/L \gtrsim 1$ is more preferable. It is remarkable that in this case the typical expected reaches

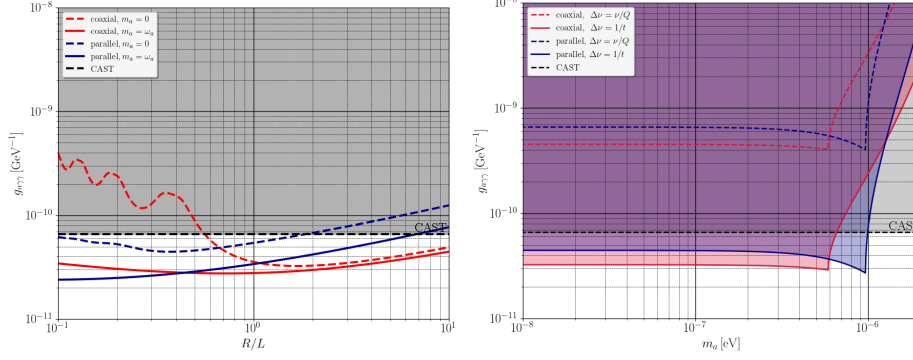


Figure 2: The sensitivity of MF emitter + M*F receiver setup for both coaxial and parallel cavity locations and the TM₀₁₀ emitter and receiver modes. Left panel: the dependence on the emitter cavity radius-to-length ratio R/L . Right panel: expected reach as a function of ALPs mass at optimal R/L for coaxial ($R/L \simeq 1.67$, $R \simeq 0.81$ m, $L \simeq 0.49$ m) and parallel ($R/L \simeq 0.37$, $R \simeq 0.49$ m, $L \simeq 1.32$ m) geometries. The integration time is $t = 10^6$ s. The temperature of the receiver is taken to be $T = 1.5$ K.

for both masses $m_a = 0$ and $m_a \simeq \omega_a$ coincide by the order of the magnitude at the level of $g_{a\gamma\gamma} \simeq 3 \times 10^{-11}$ GeV⁻¹. However, there is a notable difference between the expected reaches at $m_a = 0$ and $m_a \simeq \omega_s$ for the parallel design. Note that optimal radius to length ratio (that implies better sensitivity on $g_{a\gamma\gamma}$ in case of $m_a = 0$) is $R/L \simeq 1.67$ for coaxial design and $R/L \simeq 0.37$ for parallel design.

In Fig. 2 (right panel) we show the expected reach as a function of the ALP mass m_a for both coaxial and parallel locations of the cavities at the optimal ratios R/L assuming two options of the signal bandwidth $\Delta\nu \simeq \nu/Q_{\text{rec}}$ and $\Delta\nu \simeq 1/t$, where $t \simeq 10^6$ s is the typical time of measurement. The conservative cavity bandwidth $\Delta\nu \simeq \nu/Q_{\text{rec}}$ yields the expected limit $g_{a\gamma\gamma} \lesssim 5 \times 10^{-10}$ GeV⁻¹ that is weaker than the CAST constraint [14]. However, the optimistic bandwidth $\Delta\nu \simeq 1/t$ can provide the expected reach $g_{a\gamma\gamma} \lesssim 3 \times 10^{-11}$ GeV⁻¹ for $m_a \lesssim \omega_a/2$.

6.2 MM emitter + M*M receiver.

The second setup of our interest consists of two equal SRF cavities [10]. In the emitter cavity, ALPs are generated by an interaction of two cavity modes. In the detection cavity, produced ALPs interact with a single pump mode (which coincides with one of the production cavity pump modes), producing the resonantly enhanced signal mode in the receiver cavity. The magnitude of the surface amplitude of pump modes for an SRF cavity to be as small as $B_0^{\text{em,rec}} \lesssim 0.1$ T ($E_0^{\text{em,rec}} \lesssim 30$ MV/m) to avoid the superconductivity state destruction. The volume of the emitter and receiver cavities $V_{\text{rec}} = V_{\text{em}} \simeq 1$ m³, their quality factor $Q \simeq 10^{10}$. This high quality factor implies specific fine tuning of the emitter cavity frequency, see [15]. The expected power of the emitter cavity is $P_{\text{em}} \simeq 0.1$ kW.

In Fig. 3 (left panel) the expected reach as function of emitter radius-to-length ratio R/L is shown. We exploit $Q_{\text{rec}} = 10^{10}$ for $R/L = 1$. It turns out that the optimal magnitude of R/L for the coaxial cavity location and for the ALP mass limit $m_a = 0$ is $R/L \simeq 1.6$. The regarding expected sensitivity is $g_{a\gamma\gamma} \lesssim 5 \times 10^{-11}$ GeV⁻¹ that is comparable with the CAST bound $g_{a\gamma\gamma} \lesssim 6 \times 10^{-11}$ GeV⁻¹. For parallel location of the cavities, the optimal radius-to-length ratio is $R/L \simeq 0.35$ implying $m_a = 0$. We note that zero axion mass bounds $g_{a\gamma\gamma} \lesssim 6 \times 10^{-10}$ GeV⁻¹ are

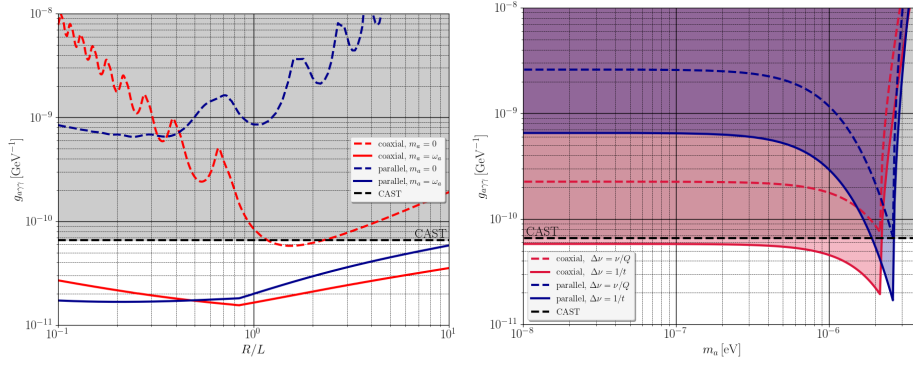


Figure 3: The sensitivity of MM emitter + M*M receiver cavity setup. This facility implies combination of TM₀₁₀ + TE₀₁₁ production pump modes. The pump mode of a receiver and its signal mode are chosen to be TM₀₁₀ and TE₀₁₁ respectively. Left panel: the expected limit $g_{a\gamma\gamma}$ as a function of production cavity radius-to-length ratio R/L (we set the emitter volume at $V_{\text{em}} = 1 \text{ m}^3$). Right panel: Sensitivity as a function of ALPs mass at optimal R/L for coaxial ($R/L \simeq 1.60$, $R \simeq 0.80 \text{ m}$, $L \simeq 0.50 \text{ m}$) and parallel ($R/L \simeq 0.35$, $R \simeq 0.48 \text{ m}$, $L \simeq 1.37 \text{ m}$) designs.

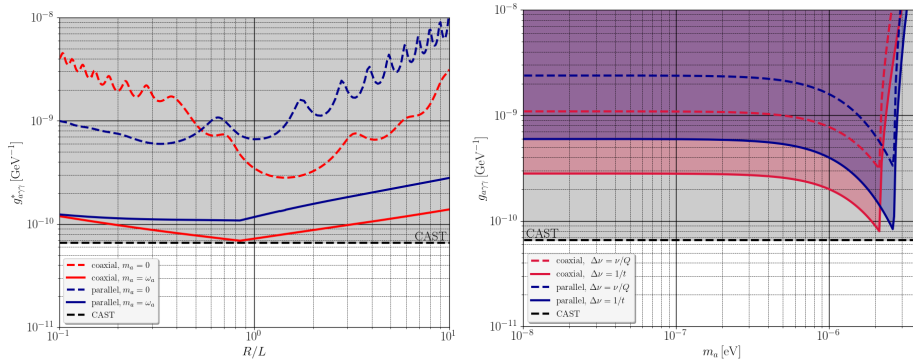


Figure 4: The sensitivity of the MM emitter + M*F receiver setup for TM₀₁₀ + TE₀₁₁ emitter pump modes and TM₀₁₀ detection signal mode. The case of ALPs frequency $\omega_a = \omega_+$ is considered. Left panel: the sensitivity dependence on emitter cavity radius-to-length ratio R/L (fixed volume of $V_{\text{em}} = 1 \text{ m}^3$ and fixed length of $L_{\text{rec}} = 0.5 \text{ m}$). Right panel: sensitivity as a function of ALPs mass at optimal R/L for coaxial ($R/L \simeq 1.44$, $R \simeq 0.77 \text{ m}$, $L \simeq 0.54 \text{ m}$, $R_{\text{rec}} \simeq 0.22 \text{ m}$, $L_{\text{rec}} \simeq 0.5 \text{ m}$) and parallel ($R/L \simeq 0.33$, $R \simeq 0.47 \text{ m}$, $L \simeq 1.43 \text{ m}$, $R_{\text{rec}} \simeq 0.18 \text{ m}$, $L_{\text{rec}} \simeq 0.5 \text{ m}$) design. Integration time is $t = 10^6 \text{ s}$, the temperature of the receiver is taken as $T = 1.5 \text{ K}$.

ruled out by the CAST. The signal cavity bandwidth is chosen to be at the level $\Delta\nu \simeq 1/t$, where $t \simeq 10^6 \text{ s}$ is a typical time of the measurements.

In Fig. 3 (right panel) we show the expected limit $g_{a\gamma\gamma}$ of this setup as a function of the ALP mass m_a . It turns out that the sensitivity has a sharp peak at the resonance $m_a \simeq \omega_a$ for both coaxial and parallel designs. For the optimistic signal bandwidth $\Delta\nu \simeq 1/t$ regarding expected limit is estimated at the level of $g_{a\gamma\gamma} \lesssim 5 \times 10^{-11} \text{ GeV}^{-1}$ for $m_a \lesssim \omega_a/2$.

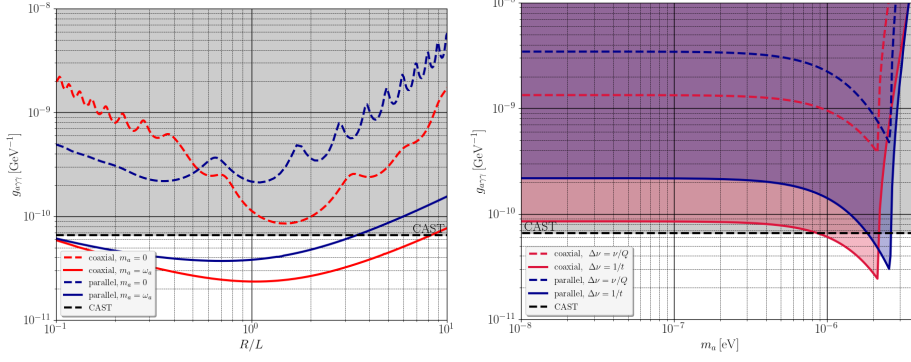


Figure 5: The sensitivity of the **MF emitter + M*M receiver** setup for TM_{010} emitter pump mode and TM_{010} receiver pump mode and TE_{011} receiver signal mode. Left panel: the sensitivity dependence on receiver cavity radius-to-length ratio R/L (fixed volume of $V_{\text{rec}} = 1 \text{ m}^3$ and fixed length of $L_{\text{em}} = 0.5 \text{ m}$). Right panel: sensitivity as a function of ALPs mass at optimal R/L for coaxial ($R/L \simeq 1.46$, $R \simeq 0.78 \text{ m}$, $L \simeq 0.53 \text{ m}$, $R_{\text{em}} \simeq 0.22 \text{ m}$, $L_{\text{em}} \simeq 0.5 \text{ m}$) and parallel ($R/L \simeq 0.36$, $R \simeq 0.49 \text{ m}$, $L \simeq 1.35 \text{ m}$, $R_{\text{em}} \simeq 0.18 \text{ m}$, $L_{\text{em}} \simeq 0.5 \text{ m}$) design. Integration time is $t = 10^6 \text{ s}$ and the temperature of the receiver is taken as $T = 1.5 \text{ K}$.

6.3 MM emitter + M*F receiver.

The next setup that we consider in our study consists of a production SRF cavity with two pump modes and a detection RF cavity immersed into static magnetic field [11, 16].

In Fig. 4 we show the sensitivity of this type of experiment for the characteristic volume of the emitter cavity $V_{\text{em}} \simeq 1 \text{ m}^3$ and its quality factor $Q_{\text{em}} \simeq 10^{10}$. Amplitudes of the emitter pump modes are $B_0^{\text{em}} = 0.1 \text{ T}$ ($E_0^{\text{em}} = 30 \text{ MV/m}$) to avoid destruction of the superconducting state. The expected power of the emitter cavity is $P_{\text{em}} \simeq 0.1 \text{ kW}$. The distance between receiver and emitter walls is $\Delta = 0.5 \text{ m}$. The pump modes of the emitter are TM_{010} and TE_{011} , and the signal mode of the receiver is TM_{010} . The receiver quality factor is $Q_{\text{rec}} \simeq 10^5$ and the typical value of the static magnetic field $B_0^{\text{rec}} = 3 \text{ T}$.

In Fig. 4 (left panel) we show the typical expected reach for this setup as a function of R/L for the emitter cavity. We emphasize that the regarding bounds are ruled out by the CAST facility at $g_{a\gamma\gamma} \lesssim 3.0 \times 10^{-10} \text{ GeV}^{-1}$. This can be also justified from the right panel of Fig. 4 where the typical bounds are shown in the $(g_{a\gamma\gamma}, m_a)$ plane.

6.4 MF emitter + M*M receiver.

The final setup consists of a production RF cavity with a pump mode into static magnetic field and a detection SRF cavity with a pump mode.

In Fig. 5 we show the sensitivity of this type of experiment for the characteristic volume of the receiver cavity $V_{\text{rec}} \simeq 1 \text{ m}^3$ and its quality factor $Q_{\text{rec}} \simeq 10^{10}$. The amplitude of the emitter pump mode is $E_0^{\text{em}} = 3 \text{ MV/m}$ ($B_0^{\text{em}} = 0.01 \text{ T}$) and the magnitude of static magnetic field is $B_{\text{ext}} = 3 \text{ T}$. The expected power of the emitter cavity is $P_{\text{em}} \sim 100 \text{ kW}$. The distance between receiver and emitter walls is $\Delta = 0.5 \text{ m}$. The pump mode of the emitter is TM_{010} , the pump mode of the receiver is TM_{010} and the signal mode of the receiver is TE_{011} . The receiver quality factor is $Q_{\text{rec}} \simeq 10^{10}$ and the typical value of the pump mode amplitude is $B_0^{\text{rec}} = 0.1 \text{ T}$.

Type of the setup	$B_0^{\text{em},(1)}$	$B_0^{\text{em},(2)}$	B_0^{rec}	Q_{rec}	P_{em}	$ \mathcal{G} $	$g_{a\gamma\gamma}$
MF em. + M*F rec.	0.01 T	3 T	3 T	10^5	100 kW	10^{-2}	$3 \times 10^{-11} \text{ GeV}^{-1}$
MM em. + M*M rec.	0.1 T	0.1 T	0.1 T	10^{10}	0.1 kW	10^{-3}	$5 \times 10^{-11} \text{ GeV}^{-1}$
MM em. + M*F rec.	0.1 T	0.1 T	3 T	10^5	0.1 kW	10^{-3}	$3 \times 10^{-10} \text{ GeV}^{-1}$
MF em. + M*M rec.	0.01 T	3 T	0.1 T	10^{10}	100 kW	10^{-3}	$9 \times 10^{-11} \text{ GeV}^{-1}$

Table 1: Table 1: Comparison of the characteristics for various experimental setups. The geometrical formfactor $|\mathcal{G}|$ and the setup sensitivity $g_{a\gamma\gamma}$ are presented for the best ratio of R/L of coaxial location and the mass of ALPs $m_a \lesssim \omega_a/2$.

In Fig. 5 (left panel) we show the typical expected reach for this setup as a function of R/L for the receiver cavity. We emphasize that the regarding bounds are ruled out by the CAST facility at $g_{a\gamma\gamma} \lesssim 9.0 \times 10^{-11} \text{ GeV}^{-1}$ for the mass range $m_a \lesssim \omega_a/2$. This can be also justified from the right panel of Fig. 5 where the typical bounds are shown in the $(g_{a\gamma\gamma}, m_a)$ plane. Remarkably however that the typical peak bounds at $m_a \simeq 2 \times 10^{-6} \text{ eV}$ can rule out the CAST limits.

7. Results and discussion.

We compared four types of the LSW radio setups for ALP searches and determined the best design for them. We summarize our study presenting important parameters for each setup in Table 1.

We concluded that the MF emitter + M*F receiver and the MM emitter + M*M receiver setups can achieve the similar top sensitivity $g_{a\gamma\gamma} \lesssim (3 - 5) \times 10^{-11} \text{ GeV}^{-1}$ at $m_a \lesssim \omega_a/2$. In particular, it turns out that the larger electromagnetic field combination and the geometrical formfactor of RF cavities compensate its smaller quality factor. Moreover, we find that the best relative location of the cavities is coaxial with the ratio of $R/L \simeq 1.6$.

The MF emitter + M*F receiver setup is a modification of the CROWS experiment [13] that implies larger volume of the cavities $V_{\text{em}} \simeq V_{\text{rec}} \simeq 1 \text{ m}^3$, lower temperature, and narrower bandwidth of the signal, $\Delta\nu \simeq 1/t$. However, there is a disadvantage of this setup that implies the relatively large emitter power $P_{\text{em}} \sim 100 \text{ kW}$. The advantage of the MM emitter + M*M receiver setup is that its emitter power is 4 orders of magnitude smaller than the previous one. Given the benchmark parameters, the last two setups, MM emitter + M*F receiver and MF emitter + M*M receiver, has the weakest sensitivity, see Table 1. Moreover, the typical bounds $g_{a\gamma\gamma} \lesssim \mathcal{O}(10^{-10}) \text{ GeV}^{-1}$ would be ruled out by the CAST.

8. Acknowledgements.

The authors thank M. Fitkevich, P. Satunin, Sergey Troitsky, Yury Senichev, and Yonatan Kahn for valuable discussions and helpful suggestions. The work is supported by RSF grant 21-72-10151.

References

- [1] R.D. Peccei and H.R. Quinn, *CP Conservation in the Presence of Instantons*, *Phys. Rev. Lett.* **38** (1977) 1440.

- [2] R.D. Peccei and H.R. Quinn, *Constraints Imposed by CP Conservation in the Presence of Instantons*, *Phys. Rev. D* **16** (1977) 1791.
- [3] J. Preskill, M.B. Wise and F. Wilczek, *Cosmology of the Invisible Axion*, *Phys. Lett. B* **120** (1983) 127.
- [4] L.F. Abbott and P. Sikivie, *A Cosmological Bound on the Invisible Axion*, *Phys. Lett. B* **120** (1983) 133.
- [5] M. Dine and W. Fischler, *The Not So Harmless Axion*, *Phys. Lett. B* **120** (1983) 137.
- [6] P. Sikivie, *Experimental Tests of the Invisible Axion*, *Phys. Rev. Lett.* **51** (1983) 1415.
- [7] A.A. Anselm, *Arion \leftrightarrow Photon Oscillations in a Steady Magnetic Field. (In Russian)*, *Yad. Fiz.* **42** (1985) 1480.
- [8] K. Van Bibber, N.R. Dagdeviren, S.E. Koonin, A. Kerman and H.N. Nelson, *Proposed experiment to produce and detect light pseudoscalars*, *Phys. Rev. Lett.* **59** (1987) 759.
- [9] F. Hoogeveen, *Terrestrial axion production and detection using RF cavities*, *Phys. Lett. B* **288** (1992) 195.
- [10] C. Gao and R. Harnik, *Axion searches with two superconducting radio-frequency cavities*, *JHEP* **07** (2021) 053 [2011.01350].
- [11] D. Salnikov, P. Satunin, D.V. Kirpichnikov and M. Fitkevich, *Examining axion-like particles with superconducting radio-frequency cavity*, *JHEP* **03** (2021) 143 [2011.12871].
- [12] Z. Bogorad, A. Hook, Y. Kahn and Y. Soreq, *Probing Axionlike Particles and the Axiverse with Superconducting Radio-Frequency Cavities*, *Phys. Rev. Lett.* **123** (2019) 021801 [1902.01418].
- [13] M. Betz, F. Caspers, M. Gasior, M. Thumm and S.W. Rieger, *First results of the CERN Resonant Weakly Interacting sub-eV Particle Search (CROWS)*, *Phys. Rev. D* **88** (2013) 075014 [1310.8098].
- [14] CAST collaboration, *New CAST Limit on the Axion-Photon Interaction*, *Nature Phys.* **13** (2017) 584 [1705.02290].
- [15] A. Romanenko et al., *New Exclusion Limit for Dark Photons from an SRF Cavity-Based Search (Dark SRF)*, *2301.11512*.
- [16] D. Salnikov, P. Satunin, D.V. Kirpichnikov and M. Fitkevich, *The Search for the Axion-Like Particles with Two Radio-Frequency Cavities*, *Moscow Univ. Phys. Bull.* **77** (2022) 145.